AGU PUBLICATIONS

Geochemistry, Geophysics, Geosystems

RESEARCH ARTICLE
10.1002/2014GC005355

Key Points:
- Arc front migration occurs globally in continental and some oceanic settings
- Crustal thickening causes arc front migration and truncates mantle melting
- Tectonic extension may balance crustal thickening for stationary arc fronts

Correspondence to:
L. Karlstrom,
leifk1@stanford.edu

Citation:
Karlstrom, L., C.-T. A. Lee, and M. Manga (2014), The role of magmatically driven lithospheric thickening on arc front migration, *Geochem. Geophys. Geosyst.*, *15*, doi:10.1002/2014GC005355.

Received 24 MAR 2014
Accepted 30 MAY 2014
Accepted article online 5 JUN 2014

The role of magmatically driven lithospheric thickening on arc front migration

L. Karlstrom[1], C.-T. A. Lee[2], and M. Manga[3]

[1]Department of Geophysics, Stanford University, Stanford, California, USA, [2]Department of Earth Science, MS-126 Rice University, Houston, Texas, USA, [3]Department of Earth and Planetary Science, University of California at Berkeley, Berkeley, California, USA

Abstract Volcanic activity at convergent plate margins is localized along lineaments of active volcanoes that focus rising magma generated within the mantle below. In many arcs worldwide, particularly continental arcs, the volcanic front migrates away from the interface of subduction (the trench) over millions of years, reflecting coevolving surface forcing, tectonics, crustal magma transport, and mantle flow. Here we show that extraction of melt from arc mantle and subsequent magmatic thickening of overlying crust and lithosphere can drive volcanic front migration. These processes are consistent with geochemical trends, such as increasing La/Yb, which show that increasing depths of differentiation correlate with arc front migration in continental arcs. Such thickening truncates the underlying mantle flow field, squeezing hot mantle wedge and the melting focus away from the trench while progressively decreasing the volume of melt generated. However, if magmatic thickening is balanced by tectonic extension in the upper plate, a steady crustal thickness is achieved that results in a more stationary arc front with long-lived mantle melting. This appears to be the case for some island arcs. Thus, in combination with tectonic modulation of crustal thickness, magmatic thickening provides a self consistent model for volcanic arc front migration and the composition of arc magmas.

1. Introduction

One of the most distinctive geographic features on Earth is the series of long arcuate chains of volcanoes on the upper plate of subduction zones, where cold and hydrothermally altered oceanic lithosphere descends into the Earth's deep interior. Arc volcanism forms one of the primary connections between long-term climate, landscape, and mantle dynamics. For example, convergent margin igneous activity is one of the main drivers of crustal differentiation and the formation of continents. Arc volcanoes create mountain ranges high and long enough to influence large-scale atmospheric circulation. They are also a significant source of volatiles, such as H_2O, CO_2, and SO_2, to the atmosphere and hydrosphere.

Surface topography, composition of erupted magmas, and the volume of volatiles released all depend on the nature of magma generation in the mantle and how these magmas interact with the upper plate. Active volcanism in subduction zones is spatially focused into a narrow, 10–30 km wide, lineament called the arc front, which varies in distance from several tens to several hundreds of kilometers from the trench. The distance of the arc front from the trench must be a manifestation of the thermal state of the mantle wedge or subducting slab and is thus of particular interest. One view is that arc magmatism is driven by hydrous flux melting of the mantle wedge, the fluids being derived from dehydration of the subducting slab as it undergoes prograde metamorphism over a narrow temperature interval [*Grove et al.*, 2009]. If arc magmatism is limited by dehydration reactions in the slab, the position of the arc front may depend primarily on the diffusive time scale for slab heating. This time scale sets the temperature structure in the overlying mantle wedge and determines whether rising melts freeze or ascend into the crust. Another view is that arc magmas originate from the hot nose of the mantle wedge, melting via decompression that is independent of dehydration reactions in the slab [*England and Katz*, 2010]. Both scenarios predict some dependency of volcano location on subduction parameters slab velocity V and dip angle δ that control flow in the wedge, and indeed, a number of studies have shown that the positions of modern arc fronts correlate negatively with slab dip or some product of slab dip and plate velocity [*Syracuse and Abers*, 2006; *Grove et al.*, 2009; *England and Katz*, 2010].

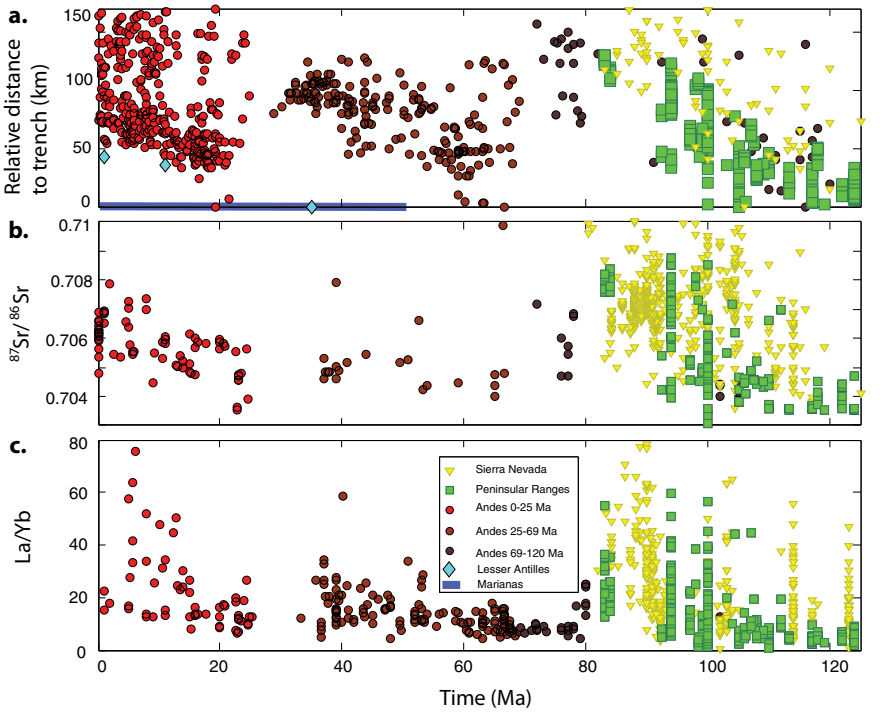

Figure 1. (a) Crystallization ages of volcanic and plutonic rocks and relative distances to the trench for three continental (Andes, Sierra Nevada, Penninsular Ranges) and two oceanic arcs (Lesser Antilles, Marianas). Andean volcanic data have been divided into three episodes and detrended to focus on the cycles of volcanic migration. Corresponding geochemical indices through time for continental arcs covary with spatial migration: (b) Initial $^{87}Sr/^{86}Sr$ isotopic ratio and (c) ratio of trace elements La/Yb.

Independent of the mechanism of melting, a longstanding extension of this correlation between subduction parameters and arc front location has been that changes in slab dip with time will move the front position relative to the trench [*Dickinson and Snyder*, 1978]. For example, the eastward migration of arc magmatism in the Sierra Nevada Batholith, California during the Late Cretaceous is widely attributed to progressive shallowing of the angle of eastward subduction of the Farallon oceanic plate beneath North America [*Coney and Reynolds*, 1977; *Dickinson and Snyder*, 1978; *Lipman*, 1992; *Humphreys et al*., 2003]. Similar arguments have been used to explain the migration of arc fronts in Tibet [*Chung et al*., 2005], Southeast China [*Li and Li*, 2007], and the Andes [*Haschke et al*., 2002]. It has also been argued that mechanical erosion by the downgoing plate may drive the migration of arc fronts [*Scholl and von Huene*, 2007].

Any successful model of subduction zones, however, must satisfy some key observations related to arc front migration. Some arcs migrate, some do not, and in those that do, migration is not always continuous (Figure 1a). Continental arc volcanism generally migrates away from the trench [*Dickinson and Snyder*, 1978], sometimes in cycles of spatial advance and retreat of volcanic activity with intervening temporal gaps in magmatism [*Haschke et al*., 2002]. Some oceanic arc fronts remain stationary relative to the trench or migrate without temporal gaps in eruptive output [*Stern et al*., 2003]. These differences appear to correspond to variations in the overall tectonic state of the overriding plate: oceanic arcs (e.g., Mariana, Tonga) are often strongly extensional, to the point of back-arc basin seafloor spreading, while some continental arcs (e.g., Andes) evolve in the presence of tectonic shortening and subduction erosion of the accretionary wedge [*Uyeda and Kanamori*, 1979; *von Huene and Scholl*, 1991].

Spatial migration of arcs also involves changes in the nature of magma transport, differentiation, and interaction with the upper plate as evidenced by evolving geochemistry as the arc front migrates. For example, the isotopic ratio $^{87}Sr/^{86}Sr$ (Figure 1b) and bulk silica content increase as continental arcs migrate away from the trench, suggesting longer magma transport times and crustal storage (we note that it is the combination of these factors that imply increased transport times rather than magma interacting with older crust). Increases in trace element ratios such as La/Yb (Figure 1c), which are sensitive to the pressure-temperature

conditions for garnet stability, suggest thickening of crust [*Haschke et al*., 2002; *Lee et al*., 2007; *DeCelles et al*., 2009].

Furthermore, in the Sierra Nevada, California, where shallowing of the slab is widely accepted to have driven migration of the arc front, xenolith data show that the Sierran arc root extended to depths of at least 90 km, approaching or even exceeding the average depth to the slab beneath modern arcs [*Ducea and Saleeby*, 1998; *Saleeby*, 2003]. This thick Sierran arc root apparently developed during the peak of arc magmatism, due to a combination of magmatic thickening and lithospheric shortening [*Barth et al*., 2012; *Chin et al*., 2012]. Thermobarometric studies indicate that this thickening root impinged directly against a normally dipping slab [*Chin et al*., 2012].

None of the above observations require that arc front migration is caused by changing dip of the downgoing slab. A number of mechanisms have been proposed for the transient flattening of slabs: subduction of oceanic plateaux [*Saleeby*, 2003], overthrusting or suction from deep continental roots [*van Hunen et al*., 2002], and evolving rheology of upper or downgoing plate [*Billen and Hirth*, 2007]. However, these mechanisms do not naturally explain the ubiquity and variability of arc front migrations or the unsteady magmatic output, and do not naturally explain the consistency between migration and geochemical data.

Here we present a new model for arc front migration. Rather than relying on time-varying dip angle of the downgoing slab, we hypothesize that arc front migration occurs by the thickening of overlying crust and lithosphere due to melt extraction from the mantle wedge. To evaluate this hypothesis, we first present a new compilation of arc front migration geochemical data that suggest thickening of crust during arc front migration. We then develop a mathematical model of arc front migration that, by including the possibility of tectonic thickening/thinning and erosive thinning of the overlying plate, can explain the presence of long-lived and stationary arc fronts in tectonic settings where large magnitude extension occurs.

We focus on the geodynamic consequences of a few interacting subduction zone components, primarily the effect of thickening or thinning the overlying plate on evolving kinematic confinement of the mantle wedge flow field. This end-member approach is similar in spirit to that which underlies the longstanding model of arc front migration as due to slab dip changes, providing a quantitative template with which to evaluate observations. In particular, this model predicts a progressively decreasing melt supply into the crust and eventual shutoff of magmatism as thickening truncates the mantle melt column, consistent with geochemical evidence for increasing magma-crust interaction over the timespan of arc front migration and eventual cessation of surface volcanism in some settings.

2. Evidence for Arc Front Migration

We compile data from five arc segments in a variety of tectonic settings, the Sierra Nevada, Peninsular Ranges, Andean, Lesser Antilles, and Izu-Bonin-Mariana arcs. These examples demonstrate both the prevalence of arc front migration and the strong variability in migration that reflects regional history.

Data for the Peninsular Ranges Batholith in Southern California were obtained from *Kistler et al*. [2003] and *Lee et al*. [2007]. The major and trace element data are based on samples averaged over a 10 by 10 foot outcrop, minimizing sampling bias (details described in *Lee et al*. [2007]). Ages are U-Pb zircon ages or Rb-Sr whole-rock isochrons. Relative distance to the trench was determined by projecting sample locations to a transect perpendicular to the current trace of the arc (the Western edge of the Coast Ranges and to the South coastal California, assuming this region represents the now extended accretionary prism). The orientation of this transect is N 51.3°E.

Data for the Sierra Nevada Batholith, California were obtained from the Navdat database based on compilations updated on 2 January 2013 (www.navdat.org). Only data for the contiguous Sierra Nevada batholith were used. Data for displaced Sierran blocks, such as the Salinia terrane, were excluded. There may be some sampling bias in this compilation because of heterogeneous sampling of the batholith in the compiled data set. Relative distance to the trench was determined by projecting sample locations to a transect perpendicular to the current trace of the arc structures and accretionary structures in the Coast Range in California. Orientation of this transect is N 48.3°E.

In both the Sierra Nevada and Peninsular Ranges Batholiths, the arc-trench distance appears to increase between 120 and 80 Ma, after which there is a sudden cessation in magmatism. Because these two arc

fronts were accompanied by emplacement of a large accretionary complex, now preserved in the California Coast Ranges and southern California "borderlands," this apparent increase in arc-trench distance is not an artifact of eroding or shortening of the leading edge of the upper plate.

Data for the Andes were taken from *Haschke et al*. [2002] for Chile between 21°S and 26°S. Unlike the Sierra Nevada and Peninsular Ranges Batholiths, the evolution of the Andean arc between 0 and 200 Ma preserves four 20–50 Myr long episodes of arc migration and compositional evolution of the arc magmas. Each of these short-term episodes appears to be characterized by gradual migration of the arc away from the trench, culminating in a magmatic gap, which in turn is followed by return of the magmatic arc toward the trench. In each episode, $^{87}Sr/^{86}Sr$ and La/Yb ratios increase, only to return to baseline values with the renewal of each cycle.

Over the 200 Myr history of the Andean arc, there appears to be a drift in the absolute location of the arc relative to the current trench [*Haschke et al*., 2002]. However, no long-term drift in the geochemistry is seen. Superimposed on a 200 Myr systematic eastward drift of the arc [*Kay and Mpodozis*, 2001; *Haschke et al*., 2002] are the shorter-term episodes of arc migration we consider to be indicative of crustal thickening. The long-term drift in absolute arc front location is likely due to subduction erosion or tectonic shortening of the western edge of the South American plate [*von Huene and Scholl*, 1991], making it difficult to know exactly the location of the arc relative to the trench in the past. We have thus normalized the beginning of each arc migration segment to a common distance specific to the given segment so that what is reported is the arc-trench distance relative to the initial arc-trench distance for a given segment of arc migration.

For the Andes, we have assumed that the orientation of the current trench relative to the past arcs has not changed. In this setting, unsteady convergence, episodes of shortening that resulted in nonmagmatic crustal thickening [*Pardo-Casas and Molnar*, 1987; *Haschke et al*., 2002], and subduction erosion [*von Huene and Scholl*, 1991] complicate the volcanic history. Despite these processes, observed trends in spatial migration and geochemistry are quite similar to the Sierran arc.

Migration data for the Lesser Antilles were compiled from the geologic map of *Macdonald et al.* [2000] and ages from *Bouysse et al*. [1990]. We have assumed that the trench location has remained constant, and study only the last 40 Ma, after the Aves ridge to the west stopped being active [*Neill et al*., 2011], and after Eocene extension in the Grenada basin ended [*Speed and Walker*, 1991; *Aitken et al*., 2011; *Manga et al*., 2012].

Data for the Izu-Bonin-Mariana come from *Stern et al*. [2003] and *Stern et al*. [2012], who argue that the arc front has maintained a nearly constant distance from the trench since the onset of magmatism after subduction initiation at ~52 Ma [*Reagan et al*., 2013]. Tectonic erosion, back-arc extension, and rotation of the trench have occurred since the inception of subduction and some migration of the volcanic front away from the trench may have occurred. However, the presence of a large ~200 km wide fore arc since the Eocene [*Stern et al*., 2012], and seafloor spreading reconstructions [*Faccenna et al*., 2009] indicate small overall motion.

Figure 2 summarizes our data compilations, an estimate for the range of probable arc front migration for the five arc segments plotted in Figure 1. Maximum and minimum migration distances and times were chosen by constructing two metrics for picking the arc front in space and time. First, we develop a point density metric for volcanism (Figure 3), which locates the highest density of activity from the trench. We then compare this location to the single closest approach of volcanism to the trench to define the error bars in Figure 2.

Our compilation is not exhaustive, and there are a number of other locations not included in this study where arc front migration away from the trench has been observed (e.g., the Cascades [*du Bray and John*, 2011], Japan [*Kimura et al*., 2005], Southeast China [*Li and Li*, 2007]), as well as those in which little migration appears to have occurred (e.g., the Aleutian arc [*Jicha et al*., 2006]), and those in uncommon tectonic environments that record more complicated migrations (e.g., trenchward migration in Nicaragua [*Plank et al*., 2002]). We however focus here on five data sets for which migration and geochemical data are most readily available, in relatively well-constrained tectonic environments. For these arc examples, Figures 1a and 2 show spatial migration of the volcanic front away from the trench is a prominent feature of the volcanic history (except for the stationary Marianas).

Although with considerable scatter, geochemical indices $^{87}Sr/^{86}Sr$ and La/Yb covary with arc position in continental arcs (Figures 1b and 1c). This scatter likely reflects the nature of available data (the Peninsular

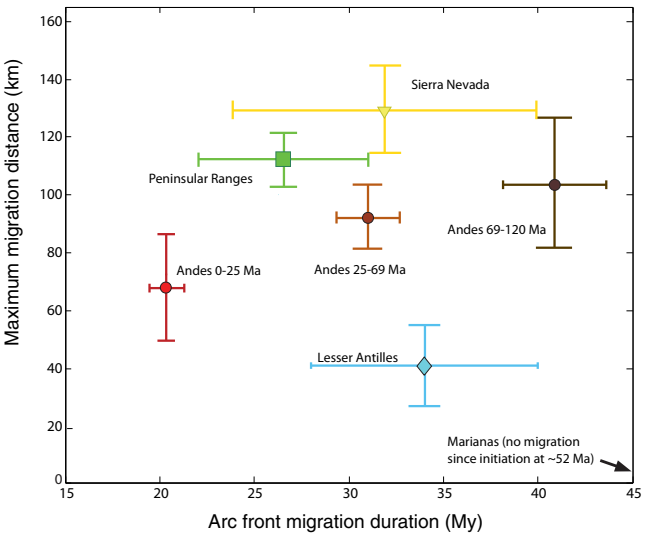

Figure 2. Observed migration times and distances for the five arcs (seven episodes) considered in this study, using spatial and temporal data from Figure 1. Error bars represent uncertainties in maximum migration times and distances discussed in text.

Ranges Batholith alone represents unbiased grid sampling) as well as our incomplete knowledge of the spatial overprinting of intrusions in time. This covariance of geochemistry with arc front position is also reflected in major elements such as bulk silica contents (a representative example from the Andes is presented later).

3. Implications for Crustal Thickening

The chemical composition of arc lavas varies systematically with crustal thickness and distance from that trench is well established [*Kuno*, 1966; *Miyashiro*, 1974]. We argue here that volcanic front migration data from a wide variety of arc settings are also consistent with crustal thickening. As Figures 1 and 2 show, in continental arcs such as the Sierra Nevada and Peninsular Ranges Batholiths, the arc front migrates away from the trench between 120 and 80 Ma, after which magmatism ceases suddenly. Because these two arc fronts were accompanied by emplacement of a large accretionary complex, this increase in arc-trench distance is not an artifact of eroding or shortening of the leading edge of the upper plate. In both cases, migration is accompanied by proxies that suggest a thickening crust: a systematic shift to higher $^{87}Sr/^{86}Sr$ and La/Yb ratios (Figure 1), the former reflecting increasing interaction with old crust in the upper plate, and the latter suggesting progressive deepening of magmatic differentiation (further supported by deeply sourced crustal xenoliths [*Chin et al.*, 2012]).

Covarying spatial migration and geochemical data suggest that migration of arc volcanism and crustal thickening might be causally related. Magmatic thickening of crust occurs via underplating, intrusions, and surface volcanic eruptions. Such crustal thickening pushes hot isotherms in the wedge away from the trench as space available for mantle circulation (already truncated by the cold region at the tip of wedge) decreases and the volume of stagnant mantle lithosphere increases. The locus of melting and melt upwelling migrates away from the trench, leading to surface arc front migration. Thickening results in longer transit times of magma rising through the crust, so erupted melts will reflect increased storage and interaction with crustal rocks during ascent. Thickening, with or without full isostatic compensation of the crust, also progressively shortens the column of mantle material available to melt and eventually shuts off melting in the wedge.

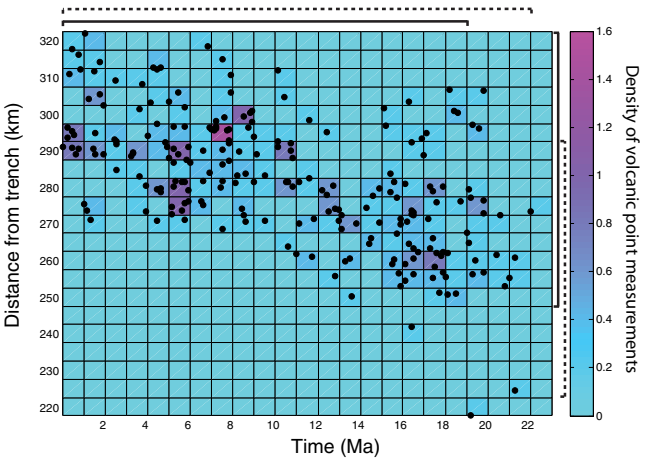

Figure 3. Example of the box counting method for determining volcanic front location in the most recent episode (0–25 Ma) of Andean arc from migration (Figure 1). We construct a point density map for each arc migration episode, using a threshold density (here 0.4 pts/(km Myr)) to determine front location (solid brackets). Upper bounds on migration are the closest points to the trench at the extrema of the episode (dashed brackets). Absolute rather than relative distance to the trench is used here.

Thus, the flux of magma into the crust decreases in time as crust thickens [*Plank and Langmuir*, 1988].

This thickening may not always be monotonic in time. For example, the Andean arc over the last 200 Ma preserves multiple episodes of arc migration and compositional evolution of the arc magmas [*Haschke et al*., 2002] (Figure 1). During each of these episodes the arc migrates gradually away from the trench, culminating in a magmatic lull, followed by return of the active magmatism toward the trench. In each episode, $^{87}Sr/^{86}Sr$ and La/Yb ratios increase, only to return to baseline values with the renewal of each cycle. Cyclic migration observed in the Andes requires a resetting of the arc front toward the trench after magmatism ceases, occurring perhaps as gravitational instabilities that remove dense lower crust [*Jull and Kelemen*, 2001] extended into the garnet stability field.

The oceanic Izu-Bonin-Mariana arc provides a contrast to continental settings in that the front-trench distance has not moved significantly since the initiation of subduction at $\sim$ 52 Ma [*Stern et al*., 2003; *Reagan et al*., 2013], even though the trench itself has rolled back to some extent [*Stern et al*., 2012]. The apparently stationary nature of this arc may be explained by the balance of magmatic thickening by back-arc extension, so that a steady state arc front location occurs with continued melting of the mantle wedge (Figure 9). Oceanic arcs with less extensive episodes of thinning through back-arc extension, such as the Lesser Antilles, exhibit more well-defined migration (Figure 1a).

4. A New Model for Volcanic Front Migration

Arc front migrations evidently illuminate a complex interplay between mantle, crustal, and surface processes that modulate arc volcanism over millions of years. Such migration has long been interpreted as the consequence of changes in the dip of the downgoing slab, and indeed the geometry of subduction will not remain static in time if the overall force balance on the slab is unsteady [*Forsyth and Uyeda*, 1975]. However, crustal thickening via melt extraction from the mantle wedge should drive arc front migration even in the absence of slab rotation and bending.

We develop a mathematical model to test whether crustal thickening, considered alongside the effects of thickening or thinning by tectonics, can explain available geochronologic and geochemical arc front migration data. We focus on upper plate processes in this model, using a simplified description of mantle flow and melting in the wedge. This approach allows us to explore the link between melting mantle, mantle flow geometry and time evolving boundary conditions.

We assume a steady state and two-dimensional subduction zone, with the distance of the volcanic front to the trench l_f set in the mantle wedge by the closest approach of the anhydrous solidus isotherm to the trench [*England et al*., 2004; *England and Katz*, 2010]. Melting occurs over a broad volume in the wedge (with or without invoking the effects of water on solidus temperatures) due to the decompression melting induced by wedge corner flow. The most trench-ward nose of these streamlines (and corresponding isotherm) provides a locus for melt focusing and ascent [*England and Katz*, 2010], while melt generated further from the trench may supply (generally lower volume) back-arc volcanism [e.g., *Till et al*., 2013]. Melt produced closer to the trench than this hot nose will generally freeze before ascending to the crust [*Grove et al*., 2012]. Thus, given a mantle flow field, changes in the boundary conditions (such as thickening of crust) will drive quasi static changes to the position of the hottest wedge isotherms and thus motion of the front position l_f.

We do not strive to model multiphase dynamics of wedge melting, neglecting nonlinear mantle rheology and downdip variability in the downgoing slab. These issues, although crucial for understanding the origins of melting and melt localization, are superimposed on the basic kinematics of subduction that drive mantle flow, decompression melting and slab dehydration. Analytic solutions to the coupled Stokes flow fluid and heat transfer problem in the mantle wedge [*England and Wilkins*, 2004] capture the basic dependence of wedge isotherms on the parameters of subduction (Figure 4a), while providing a leading-order approximation to the more general nonlinear problem.

The modeled wedge temperature field includes strong gradients in the thermal boundary layer above the slab, adiabatic temperatures in the hot core of the wedge, but no coupling to overlying crust (justified via scaling in the next section). Processes associated with unsteady motion of the downgoing plate [*Becker et al*., 1999], and finite slab width effects [*Stegman et al*., 2006; *Schellart et al*., 2007] are also ignored in this

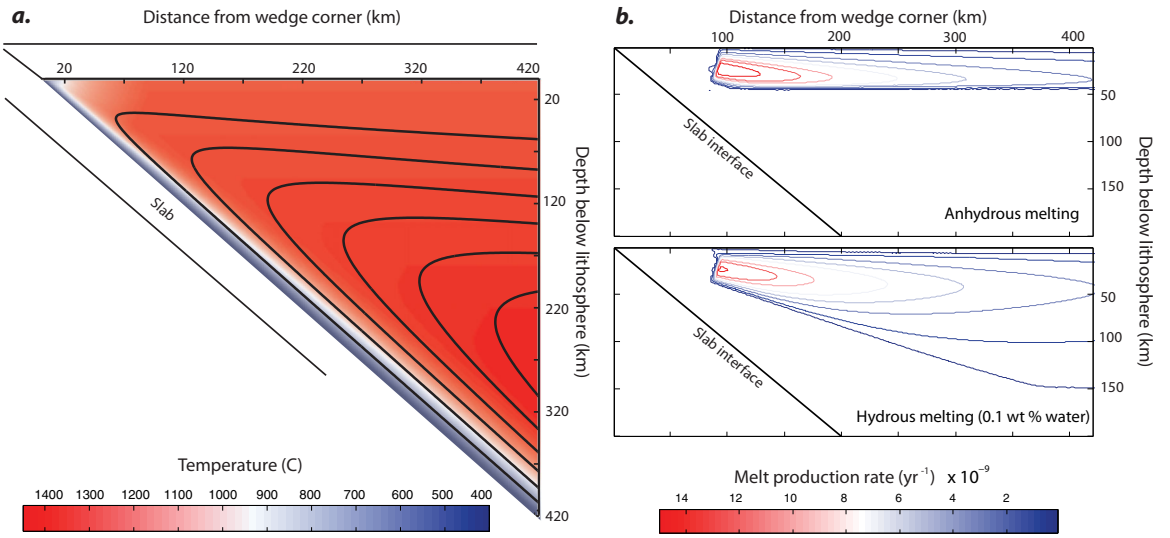

Figure 4. (a) Model mantle wedge temperature and streamlines for plate velocity $V = 10$ cm/yr and slab dip angle $\delta = 45°$. The temperature field is assumed adiabatic ($T_p = 1350°C$) away from the slab thermal boundary layer, with the top of the model domain (the colored region) representing the base of the lithosphere. (b) Melt production rate in year^{-1} for (top) anhydrous melting and (bottom) 0.1 wt % water.

study. Structure in the flow field associated with nonlinear mantle rheology, and interactions between the flow field and the growing crustal root undoubtedly add to the richness and complexity of arc front dynamics. However, validating our conceptual hypothesis requires only that melting occurs and becomes localized upon and during ascent into the overlying plate. Further, numerical treatments of the full nonlinear problem [*van Keken et al.*, 2008] must still contend with parameters for which there is considerable uncertainty but that have a large effect on predicted temperature fields and melting (such as the depth along the downgoing slab at which viscous coupling to the mantle wedge begins).

If the dependence of mantle melt focusing on subduction parameters and crustal thickness is known, arc front migration from the perspective of the overlying plate is a geometrical problem: a crustal thickness profile $Z(x, t)$ varying as a function of distance x from the trench and time t, determines the evolution of volcanic front distance to the trench $l_f(Z,t)$. With constant initial thickness crust, the front location may be obtained (symbols are illustrated in Figure 5) through

$$l_f = \frac{R\sin\delta + z_w}{\tan\delta}. \tag{1}$$

where z_w is the (constant) crustal thickness, δ the angle of subduction, and R a distance along the top of the slab to the position of the anhydrous solidus in the overlying mantle wedge flow (thus the volcanic front in this model), measured from the wedge corner [*England and Wilkins*, 2004].

From equation (1), l_f changes according to

$$\frac{dl_f(z,t)}{dt} = -(R\sin\delta + z_w\csc^2\delta)\frac{d\delta}{dt} + \frac{1}{\tan\delta}\frac{dz_w}{dt} + \cos\delta\frac{dR}{dt}, \tag{2}$$

which illustrates the contributions to volcanic front movement: the first term on the right hand side is slab bending and rotation, the second term is crustal thickening, and the third term is unsteady movement of the mantle wedge isotherm where melt focusing occurs (set by distance downslab R).

We neglect slab response or external forcing so the slab angle remains fixed, and therefore $d\delta/dt = 0$ in equation (2). However, dR/dt is not zero, because it is coupled to changes in Z (R is measured from the wedge corner so if Z or x change R must change). Equation (1) must therefore be generalized to express

this kinematic coupling. Crustal thickening will reduce the volume available to mantle flow in the wedge, which may be expressed as time variation in an angle ψ measured from the bottom interface of the over riding plate to the location of maximum plate thickness (Figure 5).

When $\psi < \delta$, equation (1) generalizes to

$$x'^2 = r^2 + (D-Z)^2 - 2R(D-Z)\cos\theta. \tag{3}$$

Here x' is the distance from the maximum of crustal thickness to the wedge corner, Z is crustal thickness (nonuniform in horizontal distance x), and θ is the angle between the top of the slab and a vertical distance D to the volcanic from l_f (Figure 5).

We simplify equation (3) by noting that

$$D = z_w + x\tan\delta, \quad l_f = x + \frac{z_w}{\tan\delta}, \quad x' = \frac{x}{\cos\phi}, \quad Z = z_w + x\tan\phi, \tag{4}$$

with z_w the initial (uniform) thickness of the overriding crust, and x the horizontal distance from the corner of the mantle wedge to the volcanic front. ϕ is an angle between the crust/mantle interface at the trench and the thickest protrusion of the overriding crust into the mantle wedge away from the trench that determines the overall volume available for flow in the wedge.

Angles in Figure 5 are related by

$$\delta = \psi + \phi, \quad \theta = \pi/2 - \delta + 2\phi, \tag{5}$$

where by assumption δ is constant. Combining equations (3–5) yields

$$0 = R^2\cos^2\phi + \left(l_f - \frac{z_w}{\tan\delta}\right)^2(\sec^2\delta\sin^2(\delta-\phi) - 1) - 2R\left(l_f - \frac{z_w}{\tan\delta}\right)\sin(\delta-2\phi)(\tan\delta - \tan\phi)\cos^2\phi. \tag{6}$$

This is the governing equation that relates volcanic front position l_f to subduction parameters and crustal thickness z through ϕ. Equation (6) reduces to equation (1) if $\phi = 0$.

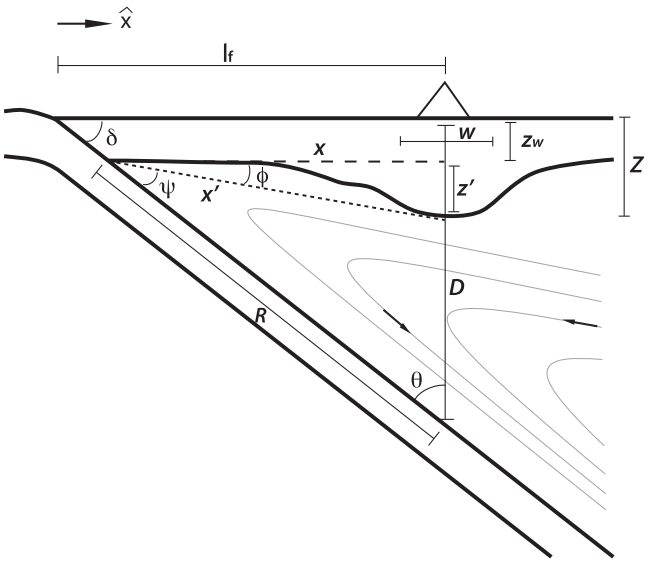

Figure 5. Geometry of the model subduction zone and crustal thickening problem, variables defined in text. Mantle wedge isotherms in thin gray lines. Localization of melting occurs around the closest approach of hot mantle wedge to the trench, whose position is determined by the dip and velocity of the downgoing slab and the thickness of overlying crust and lithosphere [*England and Katz*, 2010].

We can further reduce variables in equation (6) to only l_f and z because R depends only on ψ [*England and Wilkins*, 2004] according to

$$R = \frac{384\kappa}{\sqrt{\pi}\xi V\psi^2} + d_a|_R\tan\delta, \tag{7}$$

which may be derived by balancing the downdip thicknesses of advective and thermal boundary layers on top of the downgoing slab. In equation (7), κ is thermal diffusivity and $\xi = 1 - 2/5\sec(2\delta/5)$. ϕ is well approximated by

$$\phi = \frac{Z - z_w}{x} = \frac{Z - z_w}{l_f - z_w/\tan\delta}. \tag{8}$$

In equation (7), the second term accounts for the difference between slab perpendicular and

vertical on surface volcano location using the boundary layer d_a evaluated at the location of the volcanic front on the slab interface [*England and Wilkins*, 2004],

$$d_a|_R = \frac{64\kappa}{\sqrt{\pi}\xi V\psi}. \tag{9}$$

This is a small (<10%) correction.

Inserting equations (7) and (8) into (6) and differentiating with respect to time yields a complicated expression (reproduced in the supporting information), but it can be cast into the form

$$\frac{dl_f}{dt} = f(l_f, Z, t)\left.\frac{dZ}{dt}\right|_{x=l_f}, \tag{10}$$

relating distance of the arc front from the trench l_f to crustal thickening via the function $f(l_f,Z,t)$.

4.1. Crustal Thickening

Melt extracted from the mantle intrudes the overlying plate at Moho depths or above. We assume a constant thickness mantle lithosphere that tracks crustal thickening, and also neglect unsteady thermal evolution of the wedge during thickening. This is justified through the following scaling argument. The time scale for crustal thickening is $\tau_{thick} = \Delta z/(dZ/dt)$, where Δz is the amount of thickening and dZ/dt the thickening rate (rate of magma influx). If this time scale is longer than the relevant time scale for thermal adjustment $\tau_{therm} = \Delta d_a^2/\kappa$, with $\kappa = 0.5\times10^{-6}\mathrm{m}^2/\mathrm{s}$ thermal diffusivity, the temperature field may be considered quasistatic. As the steepest thermal gradients (and hence most wedge cooling) occurs at the top of the downgoing slab, we use as the thermal-scale distance a perturbed advective boundary layer Δd_a. Without thickening Δd_a scales as [*England and Wilkins*, 2004]

$$d_a = \left(\frac{16\kappa R^2\delta}{9\sqrt{\pi}V\xi}\right)^{1/3}, \tag{11}$$

where $\xi \approx 0.5$. We perturb R from some initial R_0 as $R \sim R_0 + \Delta z$, which assumes that perturbations to the advective boundary layer scale with perturbations to crustal thickness. Thus, $\Delta d_a = (16\kappa\Delta z^2\delta/(9\sqrt{\pi}V\xi))^{1/3}$. Taking order of magnitude parameter values $V = 10$ cm/yr, $\delta = 45^\circ$, $\Delta z = 10\mathrm{km}$, $\kappa = 0.5\times10^{-6}\mathrm{m}^2/\mathrm{s}$, and $dZ/dt = 10^{-5} - 10^{-4}\mathrm{m/yr}$ (a model result for productive arcs, described later), we find that $\tau_{thick}/\tau_{therm} \sim 10-100$, justifying our assumption of steady state. In effect, this scaling result also argues against destabilization of the growing crustal root by shear in the wedge: if the temperature field evolution is quasistatic, for long wavelength changes in Z, the wedge flow is largely governed by decreasing volume available to flow (decrease of the angle ψ in Figure 5). We will also show that thickening rate dZ/dt is a decreasing function of time and generally much less than the plate velocity V, so that the flow field is quasistatic.

We must also consider the possibility that the overlying plate thickness is not in thermal steady state at the onset of magma thickening. In general, there is a steady conductive thickening $C(x, t)$ that occurs until radiogenic heat production and heat supplied from the mantle balance growth of the thermal boundary layer. It is well known that, for oceanic plates less than 60–100 Myr in age, a simple half-space cooling model predicts the bathymetry and heat flow quite well [e.g., *Jaupart and Mareschal*, 2007]. For older plates and mature continental settings, steady state thickness may be attained and $C(x, t)$ may be negligible. Conductive thickening may occur in some arc settings [*Hall*, 2012], so we need to justify that magmatic thickening outpaces this process. We can do so by again comparing time scales: the thermal diffusion time through lithosphere of thickness Z is $\tau_{cond} = Z^2/\kappa$, while the magmatic thickening time will be somewhere between τ_{thick} defined above and $Z/(dZ/dt)$ (a time scale of ascent through the lithosphere). Taking the larger time scale of thickening with parameter values above, we find that magmatic thickening is at least 4 orders of magnitude faster than conductive thickening.

Crustal thickening thus occurs two way coupled to the mantle (thickened crust affects mantle melt flux), by magma extracted from the wedge at rate $M(x, t)$ modulated by conductive thickening $C(x, t)$, tectonic crustal forcing $T(x, t)$, and erosion $E(x, t)$ (Figure 6) as

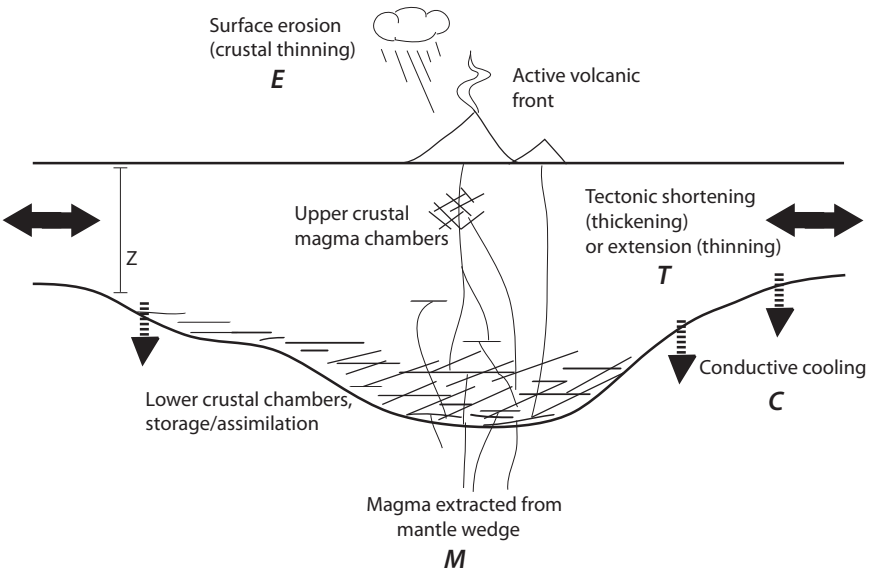

Figure 6. Processes contributing to crustal thickening in our model. We consider the local thickness $Z(x, t)$ to vary due to contributions from magmatic thickening $M(x, t)$, conductive cooling $C(x, t)$, tectonic forcing within the crust $T(x, t)$, and surface erosion $E(x, t)$.

$$\frac{dZ(x,t)}{dt} = M(x,t) + C(x,t) + T(x,t) - E(x,t). \tag{12}$$

Magmatic thickening follows from a volumetric flux of melt rising from the underlying wedge at a rate M determined by subduction parameters and mantle melt focusing mechanisms [*Sparks and Parmentier*, 1991; *England and Katz*, 2010]. Total melt in the wedge is calculated via two coupled mass conservation equations for melt and solid mantle matrix

$$\frac{\partial \rho_m F}{\partial t} + \nabla \cdot (\rho_m F \vec{U}_m) = \dot{m}, \tag{13}$$

$$\frac{\partial \rho_s (1-F)}{\partial t} + \nabla \cdot (\rho_s (1-F) \vec{U}_s) = -\dot{m}, \tag{14}$$

where ρ_m, ρ_s are melt and solid densities, $\vec{U}_m, \vec{U}_s$ are melt and solid velocities, and $\dot{m}$ is the rate of conversion between phases [*McKenzie*, 1984]. We assume steady state, constant density two phase flow, then combine these equations and integrate over the 2-D volume v of the wedge:

$$\int_v \nabla \cdot (F \vec{U}_m) dv = -\frac{\rho_s}{\rho_m} \int_v \nabla \cdot ((1-F) \vec{U}_s) dv. \tag{15}$$

Melt extraction is thus assumed to be steady state, so the left-hand side of equation (15) is the melt flux leaving the wedge that is available to thicken the crust. This neglects relative motion of the melt phase with respect to the matrix and is thus a lower bound on melt flux. The matrix velocity $\vec{U}_s = (u_r, u_\alpha)$, with (r,α) a polar coordinate system centered on the trench with angle measured from the thickest point of crust downward (maximum of α is ψ), is the analytic solution for viscous corner flow in a wedge [*Batchelor*, 1967; *McKenzie*, 1969]

$$u_r = (V(\psi \cos\psi(\alpha\cos\alpha + \sin\alpha) - \sin\psi(\alpha\cos\alpha + \sin\alpha - \psi\alpha\sin\alpha)))/(\psi^2 - \sin\psi^2). \tag{16}$$

$$u_\alpha = (V(\psi\alpha\sin\psi - \alpha + (-\psi + \alpha)\sin\psi\sin\alpha))/(\psi^2 - \sin\psi^2). \tag{17}$$

This solution neglects spatially variable viscosity.

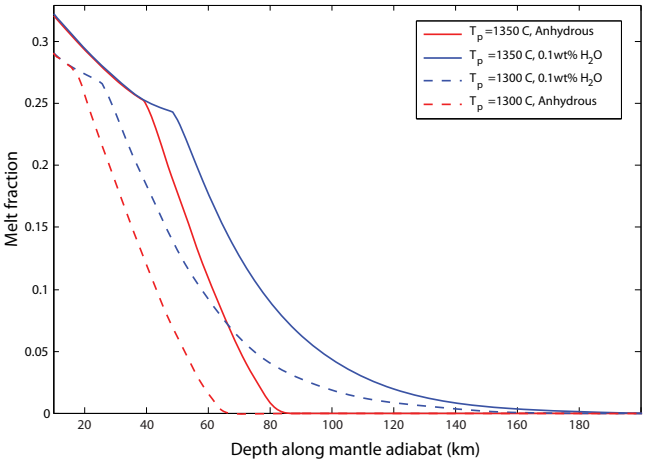

Figure 7. Calculated melt fraction along a mantle adiabat from *Katz and Spiegelman* [2003], for two choices of mantle potential temperature ($T_p = 1300°C$ dashed curves and $T_p = 1350°C$ solid curves) and water contents (red curves are anhydrous melting, blue curves are for 0.1 wt % water).

Melting is taken from the parameterization of *Katz and Spiegelman* [2003], which extends other parameterizations of adiabatic melting, for example, *Plank and Langmuir* [1992]. This model assumes adiabatically ascending mantle with a change in melt productivity after clinopyroxene is exhausted from the melting matrix. Thus, we account for the pressure, temperature, and water dependence of melting. To first order, the primary dependence of melt fraction F is on depth [*Plank and Langmuir*, 1992] (Figures 4b and 7), so most melting in our model is driven by decompression incurred by the upward sloping limb of corner flow streamlines [*Plank and Langmuir*, 1988]. Water-fluxed melting undoubtedly occurs in the mantle wedge [*Grove et al.*, 2009, 2012]; however, we assume here that its contribution to the total melt flux is superimposed on the decompression melting flux.

For completeness, we explore the dependence of melting on water content and potential temperature in Figure 7 by taking representative end-members: mantle potential temperatures of $T_p = 1300°C$ and $T_p = 1350°C$, and anhydrous melting versus mantle containing 0.1 wt % water. Assuming an average density of 3300 kg/m^3 and adiabatic gradient of 2.94×10^{-4}°C/m, we see that for anhydrous mantle, melting stops at depths below ~65 km ($T_p = 1300°C$) and ~85 km ($T_p = 1350°C$) while below ~160 and ~187 km, respectively, for hydrous melting (although the melt fraction is less than 5% at depths below 100 km for hydrous melting).

Melt focusing necessary to produce a sharp volcanic front from a horizontally broader melting region in the mantle wedge is not modeled, as we do not focus on the complexities of two phase flow in the mantle [*Sparks and Parmentier*, 1991]. Rather, we assume a Gaussian melt focusing zone centered at the volcanic front, similar to the approach taken by *England and Katz* [2010]. This gives the final form of our melt rate model

$$M(\hat{x},t)=\frac{1}{\sigma Z\sqrt{\pi}}\frac{\rho_s}{\rho_m}\left[\int_0^{\psi}\int_0^{5R}\left(\frac{(1-F)u_r}{r}+\frac{\partial}{\partial r}((1-F)u_r)+\frac{1}{r}\frac{\partial}{\partial\alpha}((1-F)u_\alpha)\right)r dr d\alpha\right]e^{-(\hat{x}-l_f)^2/(\sigma Z)^2}. \quad (18)$$

where the factor of $\sqrt{\pi}$ ensures that an integral $\int_{-\infty}^{\infty} M d\hat{x}$ equals the total melt flux in the wedge from equation (15) and σ models the width of the melt focusing region within the crust. If $F = 0$, $M = 0$ because of mass balance. We calculate the melt produced out to $5R$ here, which encompasses the entire melting region in the wedge. The distribution of melt production tails off strongly with distance from the hot nose of the wedge (Figure 4b). The presence of back-arc volcanism clearly demonstrates that melt ascends into the crust throughout this region, so our assumption of complete focusing of melt at the volcanic front is an approximation only. Letting melt ascend vertically into the overlying plate rather than focusing it toward the hot nose affects overall rates of thickening and arc front migration but not the qualitative results.

Carrying out the integration with $Z = r\sin\psi$, we find (note ψ varies with local crust thickness Z)

$$M(\hat{x},t)=\frac{V}{\sigma Z\sqrt{\pi}}\frac{\rho_s}{\rho_m}\frac{R\alpha(\psi(\psi^2-2)\sin\psi+\cos\psi(\psi^2+\sin^2\psi))}{2\psi^2-1+\cos 2\psi}e^{-(\hat{x}-l_f)^2/(\sigma Z)^2}. \quad (19)$$

When evaluated at the steady state volcanic front position [*England and Wilkins*, 2004], M is generally less than 1% of the plate velocity V.

We carry out the divergence in equation (15) to calculate melt production rate throughout the wedge. A potential temperature of $T_p = 1350°C$ results in melt production rates (integrated and averaged spatially over the entire lateral extent of wedge melting) that match qualitatively with those inferred for a variety of arc systems (20–100 km^2/Myr [*Reymer and Schubert*, 1984; *Dimalanta et al*., 2002] for representative slab parameters), and we use this for all subsequent calculations. The resulting distribution of melt production rate (in year^{-1}) is shown in Figure 4b. We see that hydrous melting extends the melt production depth, and although the melt production rate is low the overall difference in melt volumetric flux produced is ~30% (63 km^2/yr for anhydrous versus 96 km^2/yr for hydrous melting in this example).

Such differences in productivity are reflected in the rate of arc front migration and the time until a steady position is reached. As shown in Figure 8a, for the case of $V = 10$ cm/yr and $\delta = 45°$, a near-steady arc front position is achieved after ~ 120 Myr in the case of anhydrous melting but not for hydrous melting. Crustal thicknesses are predicted to increase faster and become larger in the case of hydrous melting, as melt production is higher and truncation of the melting column occurs at greater depths than for the anhydrous case (Figure 8b). Thickening rates may initially exceed ~10% of the subducting plate speed for hydrous melting, decreasing exponentially in time as the melting column shortens (Figure 8c). Further exploration of arc front migration as a function of mantle water content is outside the scope of this work, but such quantitative differences in the magnitude and duration of migration are interesting and suggest a possible route to study the mechanisms of mantle melting. We note that the early periods of highest arc front migration rate and thickening rate are the least well constrained observationally, corresponding to an assumed initiation of subduction-related volcanism in a fixed wedge geometry (~ 4 Myr in Figure 8 corresponding to subducting plate motion downdip from the trench to the distance of maximum arc front migration at 300 km).

Tectonics and erosion are assumed to scale with gravitational potential energy (local crustal thickness) as

$$T(x,t) = T_0 Z(x,t), \quad E(x,t) = E_0 Z(x,t), \tag{20}$$

where $T_0 > 0$ for compression, $T_0 < 0$ for extension, and $E_0 \geq 0$ always. These relations implicitly assume isostacy. For this exploratory purposes, we neglect erosion so $E_0 = 0$, although erosion has a similar effect to extension as formulated above. We also neglect conductive thickening $C(x, t)$ here (as our primary focus is on continental arcs) and assume constant thickness lithosphere in the absence of magmatic or tectonic effects. More generally, $C(x,t) \sim \sqrt{\kappa/t}$ from the half-space cooling solution [e.g., *Jaupart and Mareschal*, 2007] if the plate is not initially in steady state (as might be expected for oceanic arcs).

Inserting equations (19) and (20) into (12) we have

$$\frac{dZ(x,t)}{dt} = C(x,t) + M(x,t) + (T_0 - E_0)Z(x,t) = f_2(l_f, Z, \hat{x}, t), \tag{21}$$

reflecting the interplay of conductive thickening, magmatic accretion, tectonics, and erosion. We can find steady solutions to this equation if tectonics or erosion balance magmatism and conductive thickening, although we recognize that tectonics and erosion in reality are variable in space and time (T_0 and E_0 represent the rates of tectonic and erosive forcing). Here we assume constant T_0.

Given a slab angle δ and initial crustal thickness z_w plus parameters related to subduction and melting, we can thus predict the evolution of the volcanic front through two coupled ordinary differential equations

$$\frac{dl_f}{dt} = f(l_f, Z, t)\left.\frac{dZ}{dt}\right|_{\hat{x}=l_f}, \qquad \frac{dZ}{dt} = f_2(l_f, Z, \hat{x}, t). \tag{22}$$

5. Results

We numerically integrate the system of equation (22) through time using a fourth-order Runge-Kutta method. Initially, uniform thickness of overlying crust is assumed to be $z_w = 40$ km (typical for a continental setting), mantle wedge potential temperature is 1350°C [*van Keken et al*., 2002; *Lee et al*., 2009], thermal diffusivity of the wedge $\kappa = 0.5 \times 10^{-6} m^2/s$, proportionality constant between intrusion width and crust

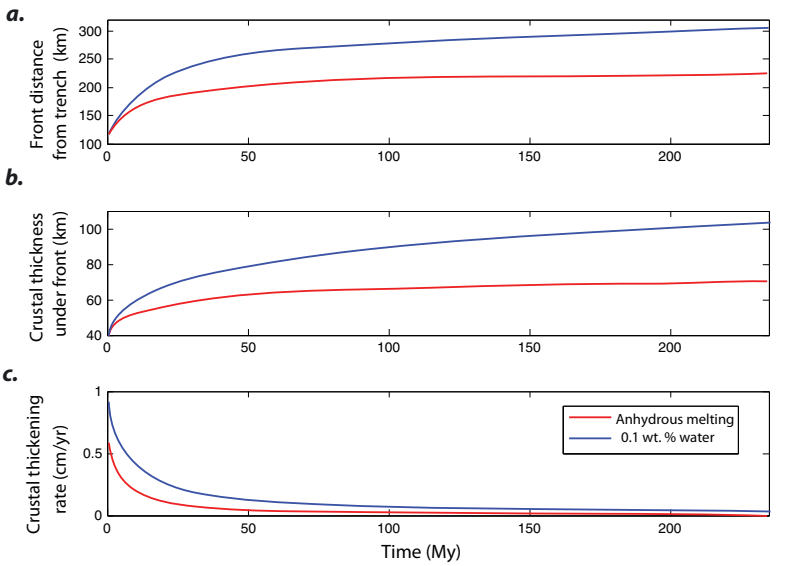

Figure 8. Example arc front migration for anhydrous (red curves) and hydrous (blue curves) mantle melting parameterizations with plate velocity $V = 10$ cm/yr and slab dip angle $\delta = 45°$. (a) Volcanic front migration away from trench. (b) Crustal thickness under front. (c) Melt addition rate (thickening) under front. Thickening rate is always less than 10% plate velocity here.

thickness $\sigma = 0.2$, and tectonic forcing in the range of $T_0 \in [-4\times10^{-7}, 4\times10^{-7}]\text{yr}^{-1}$, which spans a range of observed extensional or compressional strain rates. We use the position of the solidus isotherm [*England and Wilkins*, 2004] to determine initial volcanic front location given V and δ, and assume anhydrous melting in all cases unless otherwise noted. Simulations are run either until steady front location is reached or melting shuts off. The steady criterion is that progressive change of the volcanic front position is less than 1% per 200 kyr.

We find three distinct regimes of arc front behavior, governed by the sign and magnitude of tectonic forcing T_0. In Figure 9, we plot the crustal thickness profiles through time (time progression indicated by increasing lightness of colored curves), arc front locations, and melt production rates for three choices of T_0. In the case of no tectonic forcing ($T_0 = 0$, blue curves), thickening drives arc front migration and decreases the melt production rate in time. A steady front location is achieved when melting stops. The presence of extension on the other hand (green curves) serves to counteract thickening, such that a steady front location is reached and melting remains significant. Tectonic shortening (red curves) adds to magmatic thickening such that melting is rapidly shut off before a steady volcanic front location is achieved.

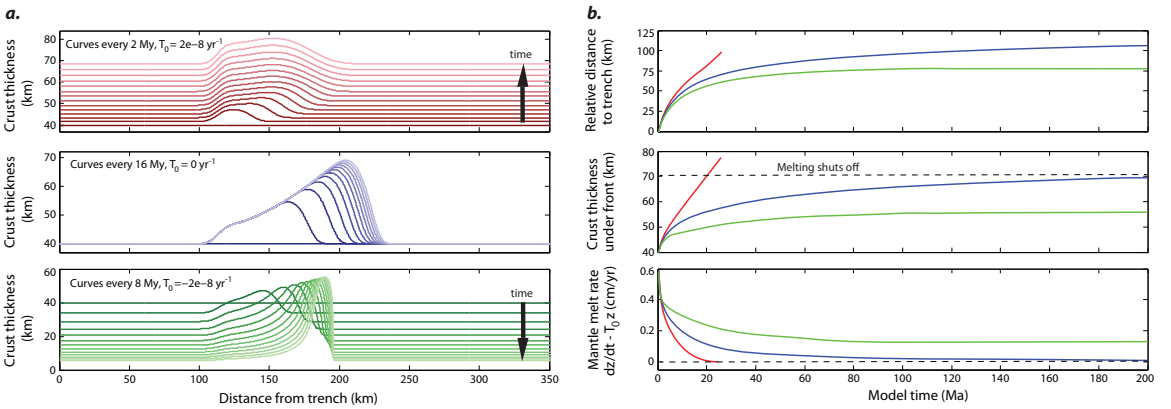

Figure 9. Predicted arc front migration during crustal thickening. (a) Crustal thickness profiles for tectonic thickening (red, $T_0 > 0$), no tectonic forcing (blue, $T_0 = 0$), and extensional thinning (green, $T_0 = 0$), time progression indicated by lighter colored curves. (b) Model behavior at the arc front, demonstrating a steady front location for extension/no tectonics, and shut off of melting for no tectonics/compression that accompanies arc front migration. Here subducting plate speed is $V = 10$ cm/yr and dip angle is $\delta = 45°$.

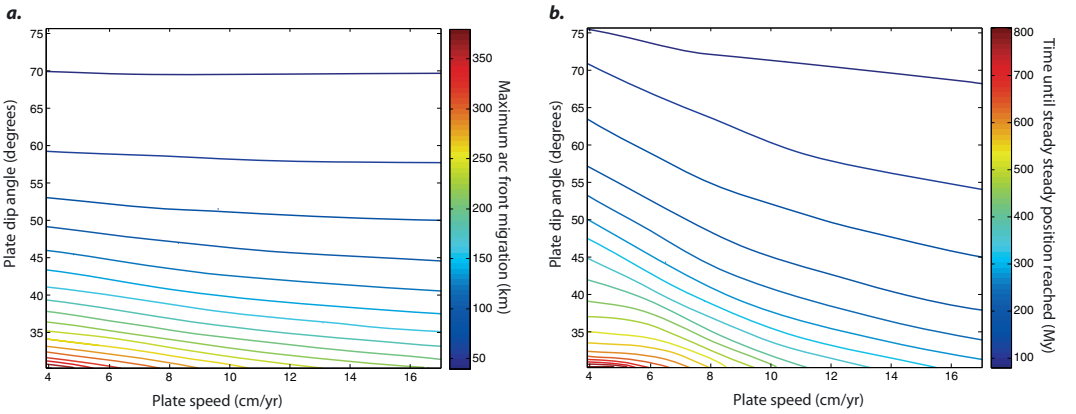

Figure 10. Model regime diagram for $T_0 = 0$ (no tectonic influence) as a function of subducting slab velocity V and slab dip angle δ. (a) Maximum migration distance (km) when steady state is reached. (b) Time until steady state (Myr), initial plate thickness 40 km.

Maximum migration distance, and the time until steady state or cessation of melting exhibit straightforward variation with subduction parameters. For negligible tectonic forcing ($T_0 = 0$) and a 40 km initial crust thickness, the regime diagram in Figure 10 shows that maximum migration time and distance are inversely correlated with slab dip angle and velocity. Slab angle is the dominant parameter, although velocity becomes increasingly important as slab dip angle decreases, especially for the migration time. This can be simply understood in terms of controls on mantle wedge melting: slab velocity sets the time scale for wedge corner flow and thus the crustal thickening rate (proportional to front migration rate), while slab angle controls the magnitude of perturbations to the corner flow volume for a given plate thickening. We do not vary the initial crustal thickness systematically here, or explicitly model oceanic settings where conductive cooling may contribute significantly to crustal thickening.

The effect of tectonic forcing magnitude is shown for a particular subduction parameter choice ($V = 10$ cm/yr, $\delta = 45°$) and 40 km initial plate thickness in Figure 11. Compression ($T_0 > 0$, blue symbols) generally results in shorter migration times than the case of no tectonics (dashed lines), as tectonically thickening the crust and lithosphere shuts off wedge melting before a steady state can be reached. Total migration distance is not significantly changed, so the predicted migration velocity in shortening environments increases. If extension ($T_0 < 0$, red symbols) outpaces melt addition and thickening, migration distances are reduced and a balance between thickening and extension is rapidly reached. As Figure 11 indicates, for some parameter choices, this results in no arc front migration at all. And in cases of extreme extension, migration toward the trench may occur as the crust at the volcanic front is thinned beyond its initial state. For all extending environments, melt production and volcanism occurs even after migration stops, as the steady state crust is not thick enough to shut off melting in the mantle wedge (thickening is balanced by extension). Oceanic arc environments that exhibit long-lived, stationary arc fronts in the presence of back-arc spreading such as the Izu-Bonin-Mariana arc [*Stern et al*., 2003; *Faccenna et al*., 2009] are qualitatively explained by this regime. Similar results are expected to hold if surface erosion rates (uniform over the domain as tectonic forcing is modeled here) exceed 0.1–1 mm/yr.

5.1. Fit With Data

It is interesting to note that the spread of observed migration distances for the five arcs studied here (30–150 km) is roughly similar to that predicted by using the average and standard deviation angle and velocity of 35 present-day subduction zones ($\delta = 49 \pm 13°$, $V = 5.9 \pm 1.9$ cm/yr, using data from *England and Katz* [2010]). Times predicted from Figure 10 are longer than migration episodes for which we have data, by over an order of magnitude in some cases. However, Figure 11c shows that addition of tectonic forcing may considerably shorten the predicted time until a steady location or melting shutoff is achieved. If mantle potential temperatures are higher than considered here, increased melting rates will also shorten the time until steady arc front location is achieved. Additionally, we find that the majority of migration and thickening occurs in the first few tens of millions of years for all parameter choices (e.g., Figures 8 and 9), so a steady position and melt shut off need not occur in all cases to match available data.

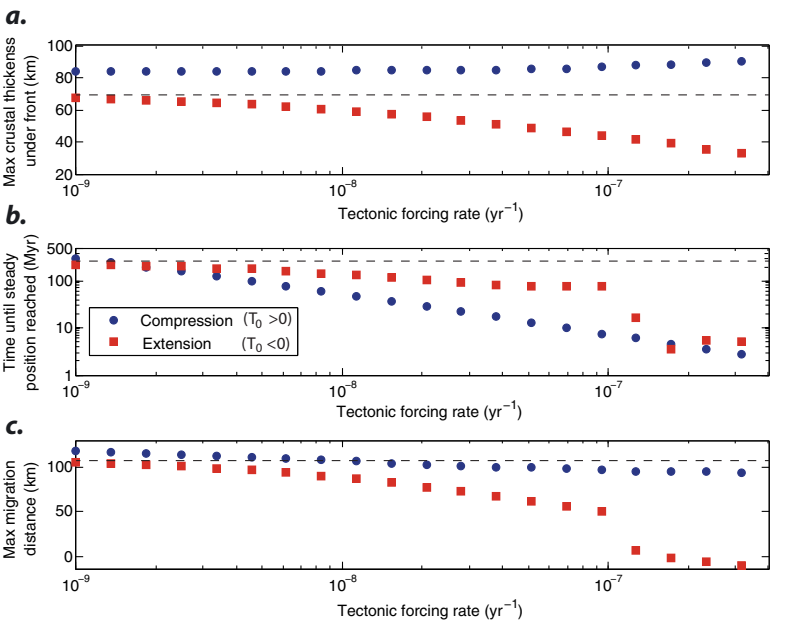

Figure 11. Effect of varying tectonic forcing T_0. Initial crustal thickness is 40 km, $V = 10$ cm/yr, $\delta = 45°$, variable tectonic forcing is $T_0 < 0$ and red squares for extension, $T_0 > 0$ and blue circles for compression. Anhydrous melting assumed. Dashed line is reference state with no tectonic forcing ($T_0 = 0$). (a) Final crustal thickness at steady state or melt shut off. (b) Time until steady state or melt shut off. (c) Maximum migration distance from trench (relative distance).

The match between predicted migration distances and data suggests that, even if slab dip angles remained static, the diversity of observed arc migrations may fit this model. Indeed, individual arc data could be inverted for the subduction history during each episode of migration as has been done using the slab flattening model [*Coney and Reynolds*, 1977]. Several complications make this step unjustified. Tectonic forcing varies significantly in time as well as space, making a simple parameterization of tectonic effects such as in Figure 11 difficult to justify for more than qualitative comparison. Hydrous melting (Figure 8) may be important, affecting the overall rate of melting and length of melting column in the wedge (leading to great migration distances and times). Subduction parameters (slab dip angle and velocity, thermal state of wedge or plates) may not remain constant for the duration of migration, and more complex coupling of the crustal root with a flow field dominated by nonlinear mantle rheology may change predicted thickening rates [*Sleep*, 2007]. Faulting and subduction erosion have variably affected estimates of relative positions of igneous activity and the original trench location, obscuring evidence for migration controlled by deeper processes on potentially different time scales and possibly contributing directly to migration [*Scholl and von Huene*, 2007].

Given these limitations, we do not attempt a systematic fit to all data in Figure 2. Future steps toward quantitative modeling of data should include arc-specific constraints on the magnitude and spatial distribution of tectonic forcing [*Oncken et al*., 2006; *Stern et al*., 2012], which will necessitate a more complete numerical treatment of mantle flow, melting and heat transfer [e.g., *Zhu et al*., 2013]. Modeling of geochemical proxies for thickening including xenolith studies [*Mantle and Collins*, 2008; *Chin et al*., 2012], and of crustal thickness [*Allmendinger et al*., 1997; *Heit et al*., 2008; *Calvert et al*., 2008] may also better constrain-specific subduction histories.

However, even assuming simple subduction geometry and spatially uniform tectonics, the crustal thickening migration model still fits the most recent arc front migration episode (from 25 Ma to the present in the Andean arc, Figure 12a). We assume no tectonic forcing ($T_0 = 0$) and constrain subduction parameters to be similar to their present day values (central Chile, $\delta = 30°$, $V = 6.7$cm/yr [*England and Katz*, 2010]), fitting the closest approach of volcanism to the present day trench. We allow for some variation in the starting time (± 2.5 Ma of the closest magmatism to the trench) and starting distance (± 10 km from the closest magmatism to the trench) to account for uncertainties in the initial position of the arc front. Geochemical trends

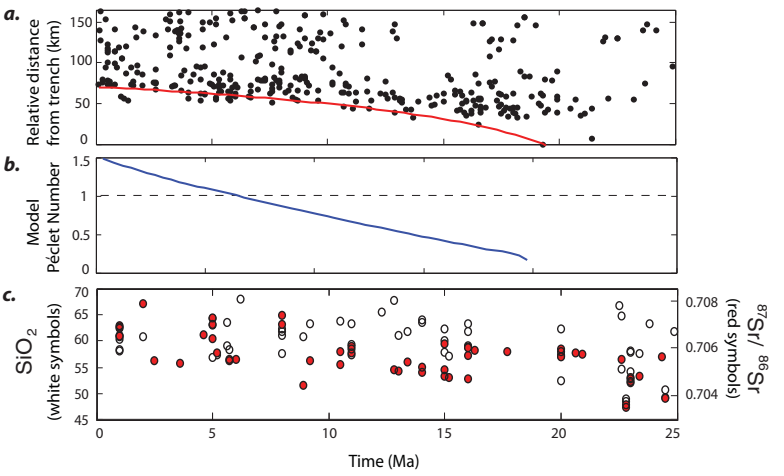

Figure 12. (a) Least squares model fit to Andean arc front migration (0–25 Ma), weighted toward nearest points to trench (exponential weight, *e*-folding distance 20 km). Best fit model parameters for $T_0 = 0$ are $V = 13$ cm/yr, $\delta = 36°$. (b) Model Péclet number defined by equation (25), illustrating transition at $Pe_c = 1$ (dashed line) from transport dominated to storage dominated magmatism as crust thickens. (c) Geochemical indices of magma differentiation (whole-rock SiO_2 in wt % and initial $^{87}Sr/^{86}Sr$ ratio) as a function of time.

are qualitatively explained by the time evolution of crustal magma transport time scales during thickening (Figures 12b and 12c), as shown in the next section.

6. Discussion

The temporal and spatial dynamics of volcanism at convergent margins reflect coupled mantle flow and melting, tectonics, surface forcing, and magma transport through a crust whose thermal and mechanical structure covaries. The robust presence of a narrow arc front structure in subduction zones globally is a remarkable signature of plate tectonics on Earth, indicating effective melt focusing over a large mantle melt catchment area. The migration of this structure in time and space with respect to the plate interface provides a window into time-varying subduction zone processes over millions of years.

We present a new model for arc front migration as an endogenic process due to mass balance between melting mantle and the crust. This model is an end-member, just as the classic model of arc front migration in terms of varying slab dip (an exogenic scenario) is an end-member, and clearly both processes may occur or interact to produce the observed volcanic vent distribution in particular arcs. However, taken alone, the crustal thickening model is attractive as it explains the observed patterns of available geochronologic and geochemical data in a variety of tectonic settings.

This model offers a myriad of predictions ranging from evolving crustal thickness profiles to mantle melt flux through time (Figure 9), in addition to the pattern of surface volcanism. More arc-specific study and detailed modeling of mantle wedge and crust dynamics will be necessary to further quantify these predictions. In addition, a global compilation of arc front migration is lacking, such that our model can not yet be tested on a truly global stage. Such a compilation for arcs in complicated tectonic settings, or those that lack significant exposures of early magmatic residua, is a nontrivial undertaking.

However, independent of such developments, it is worth considering the implication of crustal thickening-driven arc front migration on convergent margin geodynamics. Root zones that develop from crustal thickening may enhance suction on the downgoing plate and promote slab flattening [*O'Driscoll et al*., 2009]. Indeed, thickening and termination of magmatism in the Sierran arc was followed by flattening of the Farallon plate beneath much of Western North America [*Dickinson and Snyder*, 1978] (over a longer timeframe). Such changes in the mantle flow field may impart compressive stresses on the overriding plate [*DeCelles et al*., 2009], leading to shortening and promoting delamination of dense crustal root zones. Thickening may also feed back on torroidal flow generated by finite width slabs to set arc curvature [*Schellart et al*., 2007], and may vary along strike of the convergent margin. Because thickening modifies the spatial structure of the thermal field in the mantle wedge and thermal readjustment is likely quasistatic, this implies

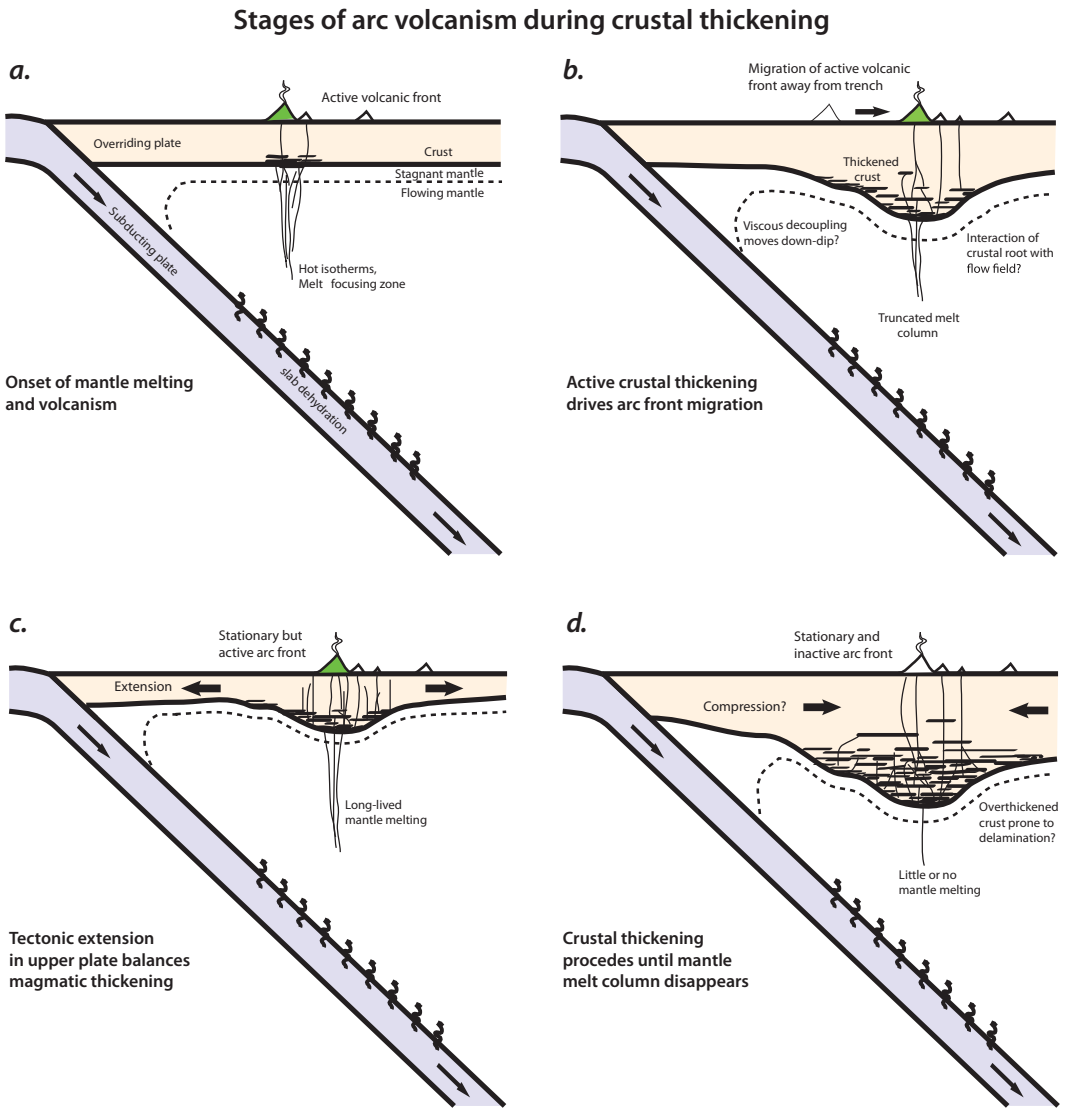

Figure 13. Conceptual model for stages of arc volcanism in the presence of crustal thickening (not time ordered). (a) Onset of focused arc magmatism with initially unmodified crust (active arc front structure in green). (b) Crustal thickening drives arc front migration while truncating the melt column at depth. (c) Stationary state in extensional environments, with steady arc front location that balances magmatic thickening with tectonic thinning. (d) Stationary state in compressional environments or those without tectonics, where crustal thickening continues until the mantle melt column is truncated, shutting off magmatism and arc front migration. The arc front is inactive.

that the region of viscous decoupling [e.g., *Wada and Wang*, 2009] between downgoing slab and wedge may migrate downdip in time as crust thickens.

There are also important implications for the time evolution of crustal magma transport (Figure 6). In a reference frame fixed to the overriding plate, melt flux into the lower lithosphere and crust decreases monotonically as crustal thickening shortens the melting column in underlying mantle. These two factors imply that the time scale for magma passage through the crust increases according to

$$\tau_m = \frac{Z}{dZ/dt}, \tag{23}$$

with dZ/dt the crustal thickening rate. Magma ascent may depart from this time scale depending on the mode of transport and storage in magma chambers. However, the compositional and rheological stratification of the crust generally promote intrusion rather than surface eruption, as evidenced by widespread

intrusive to extrusive ratios larger than unity (even without taking into account mafic melt addition to the lower crust [*White et al*., 2006]). Thus, lengthening τ_m increases the enthalpy delivered to the crust by intrusions, heating the crust and increasing the stability of crustal storage zones [*Dufek and Bergantz*, 2005; *Karlstrom et al*., 2010]. The crustal maturation represented by the thermal and mechanical stability of long-lived and compositionally evolved magma reservoirs is controlled by the ratio of elastic to viscoelastic response time scales (a Deborah number De) in crustal rocks surrounding intrusions,

$$\mathrm{De} = \frac{\tau_{maxwell}}{\tau_{elastic}} = \frac{\mu_{cr}/Y}{V_{ch}/Q}, \tag{24}$$

where V_{ch} is the chamber volume, Q is the incoming magma flux, μ_{cr} is the host rock viscosity, and Y is the Young's Modulus of host rocks. This ratio must be less than unity for magma storage without eruption, and may be cast equivalently as a Péclet number that measures the relative importance of magma addition versus heat dissipation to crustal rocks [*Karlstrom et al*., 2010]. We assume that magma flux Q and hence $\tau_{elastic}$ scale inversely with τ_m, while diffusion scales with the typical length scales of intrusions. If we then consider intrusions that scale with arc front widths $W = 10$–30 km, we might expect that at a location $\hat{x}$ of the volcanic front the quantity

$$\mathrm{Pe}_c(\hat{x}) = \frac{\tau_m}{\tau_d} = Z(\hat{x},t)\left(\frac{dZ(\hat{x},t)}{dt}\right)^{-1}\frac{\kappa}{W^2}, \tag{25}$$

controls the mode of magma storage, with a transition from advection to storage dominated magma transport as Pe_c increases through order unity.

This behavior is shown in Figure 12b for $W = 20$ km, with model Péclet number transitioning through order unity $\sim$ 15 million years after the onset of migration. Although we do not model geochemical evolution explicitly, Figure 12c illustrates that the differentiation trends in SiO_2 and $^{87}Sr/^{67}Sr$ isotopes mimic the increase in Péclet number as crust thickens. Such trends are common and widely recognized in the increasing proportion of calc-alkalic series volcanic rocks with increasing continental character of arcs as well as with distance from the trench [*Kuno*, 1966; *Miyashiro*, 1974].

Increased transit and storage times imply that crustal rheology evolves during arc front migration, as heat is conducted from rising magma to surrounding crustal rocks [*Hildreth and Moorbath*, 1988; *Dufek and Bergantz*, 2005]. This in turn may result in an increased fraction of intruded to erupted magmas throughout the period of active magmatism: warming country rocks, and progressively decreasing melt supply due to crustal thickening, should lead to stable storage and viscous accommodation of intruded magmas [*Karlstrom et al*., 2010; *Karlstrom and Richards*, 2011]. This could result in less frequent, more chemically evolved and larger volume individual surface eruptions as the arc matures, with increasing surface heat flow due to larger volumes of intrusions. The growth of a deep crustal, possibly sulfide-rich, cumulate reservoir [*Lee et al*., 2012] would imply a source of ore metals in the upper plate in addition to fluids rising from the subducting slab [*Kay and Mpodozis*, 2001], perhaps explaining trench parallel metallogenic provinces in the Andes, southern China and western North America [*Wang et al*., 2011]. Finally, migration of the arc front and storage of rising magmas could prolong metamorphic decarbonation of carbonated sediments in the upper plate, maintaining steady volcanic climate forcing over tens of millions of years where migration occurs [*Lee et al*., 2013].

7. Conclusions

Data compiled from arcs in several continental settings suggest that arc front migration away from the trench is a general feature of the arc magmatic life cycle (Figure 1). Migration ends either in the cessation of magmatism (Sierras, Peninsular Ranges), or proceeds as part of a broader cycle in which the arc front position resets back toward the trench after migration occurs (Andes). In oceanic arcs, the situation is more complex, and we have shown that some oceanic arc fronts migrate (Lesser Antilles), while as others appear to have long-lived but stationary arc fronts (Marianas). Stationarity appears to coincide with the presence of extensional tectonics in the overlying plate [*Stern et al*., 2012]. Geochemical indices consistent with

progressive crustal thickening track the spatial migration of arc fronts in settings where such data are available (continental arcs). Based on this evidence and point measurements of P-T-t histories from mantle xenoliths [*Chin et al*., 2012], we suggest that crustal thickening plays a significant role in arc front migration.

This model differs from the traditional interpretation of arc front migration caused by slab flattening. If correct, the migration of the arc front is a unique proxy for the interaction between evolving crust, the mantle flow field and mantle melting over millions of years. We summarize the arc life cycle implied by this model in four general system states, visited at different times by different arcs (or not at all) depending on local conditions (Figure 13). At the onset of subduction-related mantle melting and crustal magma transport (Figure 13a), crust is unmodified by ascending melt, and mantle wedge flow is set by the kinematics of subduction initiation. As crustal thickening proceeds (Figure 13b), this drives arc front migration as mantle wedge material is squeezed away from the trench. During this stage, magmatic inflation of the crust by intrusions and surface eruptions are the dominant forcings on the overlying plate. Isotherms that control melt focusing and the thermal/rheological structure of the forearm mantle migrate away from the trench. Thickening crust progressively truncates the mantle melt column, causing decreasing melt production through time.

In settings where tectonic extension in the overlying plate balances magmatic thickening (Figure 13c), long-lived mantle melting can occur and stationary arc fronts are the result. If crustal thickening due to magmatism (or tectonic thickening, or conductive cooling) dominates (Figure 13d), the mantle melt column becomes so shortened that no surface volcanism can occur and the arc is inactive. However, over thickened crust may extend into the stability field of dense phases such as garnet and be prone to density instabilities that might reset melting and the arc front position back toward the trench.

Acknowledgments
We thank Bob Stern and an anonymous reviewer as well as Editor Thorsten Becker for constructive comments that have improved the manuscript. We acknowledge support from an NSF postdoctoral fellowship (Karlstrom), and the NSF FESD program (Lee and Manga). Data used in this work are available from the sources cited in the text (geochemical and geochronologic data) and supplement (analytic expressions too lengthy for the main text).

References

Aitken, T., P. Mann, A. Escalona, and G. Christeson (2011), Evolution of the Grenada and Tobago basins and implications for arc migration, *Mar. Pet. Geol.*, *28*, 235–258.
Allmendinger, R., T. Jordan, S. Kay, and B. Isacks (1997), The evolution of the Altiplano-Puna plateau of the Central Andes, *Annu. Rev. Earth Planet. Sci.*, *25*, 139–174.
Barth, A., J. Wooden, C. Jacobson, and R. Economos (2012), Detrital zircon as a proxy for tracking the magmatic arc system: The California arc example, *Geology*, *41*(2), 223–226.
Batchelor, G. K. (1967), *An Introduction to Fluid Dynamics*, Cambridge Univ. Press.
Becker, T., C. Faccenna, R. O'Connell, and D. Giardini (1999), The development of slabs in the upper mantle: Insights from numerical and laboratory experiments, *J. Geophys. Res.*, *104*(B7), 15,207–15,226.
Billen, M., and G. Hirth (2007), Rheologic controls on slab dynamics, *Geochem. Geophys. Geosyst.*, *8*, Q08012, doi:10.1029/2007GC001597.
Bouysse, P., D. Westercamp, and P. Andrieff (1990), The Lesser Antilles island arc, *Proc. Ocean Drill. Program Sci. Results*, *110*, 29–44.
Calvert, A. J., S. Klemperer, N. Takahashi, and B. Kerr (2008), Three-dimensional crustal structure of the Mariana island arc from seismic tomography, *J. Geophys. Res.*, *113*, B01406, doi:10.1029/2007JB004939.
Chin, E., C.-T. Lee, P. Luffi, and M. Tice (2012), Deep lithospheric thickening and refertilization beneath continental arcs: Case study of the p, t and compositional evolution of peridotite xenoliths from the Sierra Nevada, California, *J. Petrol.*, *53*, 477–511.
Chung, S.-L., M.-F. Chu, Y. Zhang, Y. Xie, C.-H. Lo, C.-T. Lee, C.-Y. Lan, X. Li, Q. Zhang, and Y. Wang (2005), Tibetan tectonic evolution inferred from spatial and temporal variations in post-collisional magmatism, *Earth Sci. Rev.*, *68*, 251–257.
Coney, P., and S. Reynolds (1977), Cordilleran Benioff zones, *Nature*, *279*, 403–406.
DeCelles, P., M. Ducea, P. Kapp, and G. Zandt (2009), Cyclicity in Cordilleran orogenic systems, *Nat. Geosci.*, *2*, 251–257.
Dickinson, W. R., and W. S. Snyder (1978), Plate tectonics of the Laramide orogeny, in *Laramide Folding Associated With Basement Block Faulting in the Western United States*, edited by V. Matthews, pp. 355–366, Geol. Soc. of Am.
Dimalanta, C., A. Taira, G. P. Yumul Jr., H. Tokuyama, and K. Mochizuki (2002), New rates of western Pacific island arc magmatism from seismic and gravity data, *Earth Planet. Sci. Lett.*, *202*, 105–115.
du Bray, E., and D. John (2011), Petrologic, tectonic, and metallogenic evolution of the ancestral cascades magmatic arc, washington, oregon, and northern california, *Geosphere*, *7*, 1102–1133.
Ducea, M., and J. Saleeby (1998), The age and origin of a thick mafic-ultramafic keel from beneath the Sierra Nevada batholith, *Contrib. Mineral. Petrol.*, *133*, 169–185.
Dufek, J., and G. W. Bergantz (2005), Lower crustal magma genesis and preservation: A stochastic framework for the evaluation of basalt-crust interaction, *J. Petrol.*, *46*(11), 2167–2195.
England, P., and R. Katz (2010), Melting above the anhydrous solidus controls the location of volcanic arcs, *Nature*, *467*, 700–704.
England, P., and C. Wilkins (2004), A simple analytical approximation to the temperature structure in subduction zones, *Geophys. J. Int.*, *159*, 1138–1154.
England, P., R. Engdahl, and W. Thatcher (2004), Systematic variations in the depths of slabs beneath arc volcanoes, *Geophys. J. Int.*, *156*, 377–408.
Faccenna, C., E. Giuseppe, F. Funiciello, S. Lallemand, and J. van Hunen (2009), Control of seafloor aging on the migration of the Izu-Bonin-Marian trench, *Earth Planet. Sci. Lett.*, *288*(3-4), 386–398.
Forsyth, D., and S. Uyeda (1975), On the relative importance of the driving forces of plate motion, *Geophys. J. R. Astron. Soc.*, *43*, 163–200.
Grove, T., C. Till, E. Lev, N. Chatterjee, and E. Medard (2009), Kinematic variables and water transport control the formation and location of arc volcanoes, *Nature*, *459*, 694–697.
Grove, T., C. Till, and M. Krawczynski (2012), The role of H_2O in subduction zone magmatism, *Annu. Rev. Earth Planet. Sci.*, *40*, 413–439.
Hall, P. (2012), On the thermal evolution of the mantle wedge at subduction zones, *Phys. Earth Planet. Inter.*, *198–199*, 9–27.

Haschke, M., E. Scheuber, D. Gunther, and K.-J. Reutter (2002), Evolutionary cycles during Andean orogeny: Repeated slab breakoff and flat slab subduction?, *Terra Nova*, *14*, 49–55.
Heit, B., X. Yuan, M. Bianchi, F. Sodoudi, and R. Kind (2008), Crustal thickness estimation beneath the southern Central Andes at 30 S and 36 S from S wave receiver function analysis, *Geophys. J. Int.*, *174*, 249–254.
Hildreth, W., and S. Moorbath (1988), Crustal contributions to arc magmatism in the Andes of Central Chile, *Contrib. Mineral. Petrol.*, *98*, 455–489.
Humphreys, E., E. Hessler, K. Dueker, G. Farmer, E. Erslev, and T. Atwater (2003), How Laramide-age hydration of North American lithosphere by the Farallon slab controlled subsequent activity in the western United States, *Int. Geol. Rev.*, *45*, 575–595.
Jaupart, C., and J.-C. Mareschal (2007), Constraints on crustal heat production from 863 heat flow data, in Treatise of Geochemistry: The Crust, edited by R. L. Rudnick, 864, pp. 65–84, Elsevier Science Publishers, Amsterdam.
Jicha, B., D. Scholl, B. Singer, and G. Yogozinski (2006), Revised age of Aleutian Island Arc formation implies high rate of magma production, *Geology*, *34*(8), 661–664.
Jull, M., and P. Kelemen (2001), On the conditions for lower crustal convective instability, *J. Geophys. Res.*, *106*(B4), 6423–6446.
Karlstrom, L., and M. Richards (2011), On the evolution of large ultrmafic magma chambers and timescale for flood basalt eruptions, *J. Geophys. Res.*, *116*, B08216, doi:10.1029/2010JB008159.
Karlstrom, L., J. Dufek, and M. Manga (2010), Magma chamber stability in arc and continental crust, *J. Volcanol. Geotherm. Res.*, *190*, 249–270.
Katz, R., and M. Spiegelman (2003), A new parameterization of hydrous mantle melting, *Geochem. Geophys. Geosyst.*, *4*(9), 1073, doi: 10.1029/2002GC000433.
Kay, S., and C. Mpodozis (2001), Central Andean ore deposits linked to evolving shallow subduction systems and thickening crust, *GSA Today*, *11*, 4–9.
Kimura, J.-I., R. J. Stern, and T. Yoshida (2005), Reinitiation of subduction and magmatic responses in SW Japan during Neogene time, *Geol. Soc. Am. Bull.*, *117*(7-8), 969–986.
Kistler, R., J. Wooden, and D. Morton (2003), Isotopes and ages in the northern Peninsular Ranges batholith, Southern California, *U.S. Geol. Surv. Open File Rep., 03–489*, 45.
Kuno, H. (1966), Lateral variation of basalt magma type across continental margins and island arcs, *Bull. Volcanol.*, *29*, 195–222.
Lee, C.-T., D. Morton, R. Kistler, and A. Baird (2007), Petrology and tectonics of phanerozoic continent formation: From Island arcs to accretion and continental arc magmatism, *Earth Planet. Sci. Lett.*, *263*, 370–387.
Lee, C.-T., P. Luffi, T. Plank, H. Dalton, and W. Leeman (2009), Constraints on the depths and temperatures of basaltic magma generation on Earth and other terrestrial planets using new thermobarometers for mafic magmas, *Earth Planet. Sci. Lett.*, *279*, 20–33.
Lee, C.-T., P. Luffi, E. Chin, R. Bouchet, R. Dasgupta, D. Morton, V. L. Roux, Q.-Z. Yin, and D. Jin (2012), Copper systematics in arc magmas and implications for crust-mantle differentiation, *Science*, *336*, 64–68.
Lee, C.-T., et al. (2013), Continental arc-island arc fluctuations, growth of crustal carbonates, and long-term climate change, *Geosphere*, *9*(1), 21–36.
Li, Z.-X., and Z.-H. Li (2007), Formation of the 1300-km wide intracontinental orogen and postorogenic magmatic province in Mesozoic South China: A flat-slab subduction model, *Geology*, *35*, 179–182.
Lipman, P. W. (1992), Magmatism in the Cordilleran United States; progress and problems, in *The Geology of North America, vol G3, The Cordilleran Orogen, Conterminous U.S.*, edited by B. C. Burchfiel, P. W. Lipman, and M. L. Zoback, pp. 481–514, Geol. Soc. of Am. Boulder Co.
Macdonald, R., C. Hawkesworth, and E. Heath (2000), The Lesser Antilles volcanic chain: A study in arc magmatism, *Earth Sci. Rev.*, *49*, 1–76.
Manga, M., et al. (2012), Heat flow in the Lesser Antilles island arc and adjacent back arc Grenada basin, *Geochem. Geophys. Geosyst.*, *13*, Q08007, doi:10.1029/2012GC004260.
Mantle, G., and W. Collins (2008), Quantifying crustal thickness variations in evolving orogens: Correlation between arc basalt compositon and moho depth, *Geology*, *36*, 87–90.
McKenzie, D. (1969), Speculations on the consequences and causes of plate motion, *Geophys. J. R. Astron. Soc.*, *18*, 1–32.
McKenzie, D. (1984), The generation and compaction of partially molten rock, *J. Petrol.*, *25*(3), 713–765.
Miyashiro, A. (1974), Volcanic rock series in island arcs and active continental margins, *Am. J. Sci.*, *274*, 321–355.
Neill, I., A. Kerr, A. Hastie, K.-P. Stanek, and I. Millar (2011), Origin of the Aves ridge and Dutch-Venezuelan Antilles: Interaction of the cretaceous 'Great Arc' and Caribbean-Colombian oceanic plateau?, *J. Geol. Soc.*, *168*(2), 333–348.
O'Driscoll, L., E. Humphreys, and F. Saucier (2009), Subduction adjacent to deep continental roots: Enhanced negative pressure in the mantle wedge, mountain building and continental motion, *Earth Planet. Sci. Lett.*, *280*, 61–70.
Oncken, O., D. Hindle, J. Kley, K. Elger, P. Victor, and K. Schemmann (2006), Deformation of the Central Andean upper plate system—Facts, fiction, and constraints for plateau models, in *The Andes: Actice Subduction Orogeny*, edited by O. Oncken et al., chap. 1, Springer.
Pardo-Casas, F., and P. Molnar (1987), Relative motion of the Nazca (Farallon) and South American plates since Late Cretaceous time, *Tectonics*, *6*(3), 233–248.
Plank, T., and C. Langmuir (1988), An evaluation of the global variations in the major element chemistry of arc basalts, *Earth Planet. Sci. Lett.*, *90*, 349–370.
Plank, T., and C. Langmuir (1992), Effects of the melting regime on the composition of the oceanic crust, *J. Geophys. Res.*, *97*(B13), 19,749–19,770.
Plank, T., V. Balzer, and M. Carr (2002), Nicaraguan volcanoes record paleoceanographic changes accompanying closure of the Panama gateway, *Geology*, *30*(12), 1087–1090.
Reagan, M., W. McClelland, G. Girard, K. Goff, D. Peate, Y. Ohara, and R. Stern (2013), The geology of the southern mariana fore-arc crust: Implications for the scale of Eocene volcanism in the western Pacific, *Earth Planet. Sci. Lett.*, *380*, 41–51.
Reymer, A., and G. Schubert (1984), Phanerazoic addition rates to the continental crust and crustal growth, *Tectonics*, *3*(1), 63–77.
Saleeby, J. (2003), Segmentation of the Laramide slab–Evidence from the southern Sierra Nevada, *Geol. Soc. Am. Bull.*, *115*, 655–668.
Schellart, W., J. Freeman, D. Stegman, L. Moresi, and D. May (2007), Evolution and diversity of subduction zones controlled by slab width, *Nature*, *446*, 308–311.
Scholl, D., and R. von Huene (2007), Crustal recycling at modern subduction zones applied to the past–issue of growth and preservation of continental basement crust, mantle geochemistry, and supercontinent reconstruction, *Geol. Soc. Am. Mem.*, *200*, 9–32.
Sleep, N. (2007), Edge-modulated stagnant-lid convection and volcanic passive margins, *Geochem. Geophys. Geosyst.*, *8*, Q12004, doi:10.1029/2007GC001672.
Sparks, D., and E. Parmentier (1991), Melt extraction from the mantle beneath spreading centers, *Earth Planet. Sci. Lett.*, *105*, 368–377.
Speed, R., and J. Walker (1991), Oceanic-crust of the Grenada basing in the southern Lesser Antilles arc platform, *J. Geophys. Res.*, *96*(B3), 3835–3851.

Stegman, D., J. Freeman, W. Shellart, L. Moresi, and D. May (2006), Influence of trench width on subduction hinge retreat rates in 3-d models of slab rollback, *Geochem. Geophys. Geosyst.*, *7*, Q03012, doi:10.1029/2005GC001056.

Stern, R., M. Fouch, and S. Klemperer (2003), An overview of the Izu-Bonin-Mariana subduction factory, *Geophys. Monogr.*, *138*, 175–222.

Stern, R., M. Reagan, O. Ihizuda, Y. Ohara, and S. Whattam (2012), To understand subduction initiation, study forearc crust: To understand forearc crust, study ophiolites, *Lithosphere*, *4*, 469–483, doi:10.1130/L183.1.

Syracuse, E., and G. Abers (2006), Global compilation of variations in slab depth beneath arc volcanoes and implications, *Geochem. Geophys. Geosyst.*, *7*, Q05017, doi:10.1029/2005GC001045.

Till, C., T. Grove, R. Carlson, R. Donnelly-Nolan, J. Fouch, L. Wagner, and W. Hart (2013), Depths and temperatures of $<$10.5 ma mantle melting and the lithosphere-asthenosphere boundary below southern oregon and northern california, *Geochem. Geophys. Geosyst.*, *14*, 864–879, doi:10.1002/ggge.20070.

Uyeda, S., and H. Kanamori (1979), Back-arc opening and the mode of subduction, *J. Geophys. Res.*, *84*(B3), 1049–1061.

van Hunen, J., A. van den Berg, and N. Vlaar (2002), On the role of subducting oceanic plateaus in the development of shallow flat subduction, *Tectonophysics*, *352*(3-4), 317–333.

van Keken, P., B. Kiefer, and S. Peacock (2002), High resolution models of subduction zones: Implications for mineral dehydration reactions and the transport of water into the deep mantle, *Geochem. Geophys. Geosyst.*, *3*(10), 1056, doi:10.1029/2001GC000256.

van Keken, P., et al. (2008), A community benchmark for subduction zone modeling, *Phys. Earth Planet. Inter.*, *171*, 187–197.

von Huene, R., and D. Scholl (1991), Observations at convergent margins concerning sediment subduction, subduction erosion, and the growth of continental crust, *Rev. Geophys.*, *29*, 279–316.

Wada, I., and K. Wang (2009), Common depth of slab-mantle decoupling: Reconciling diversity and uniformity of subduction zones, *Geochem. Geophys. Geosyst.*, *10*, Q10009, doi:10.1029/2009GC002570.

Wang, F.-Y., M.-X. Ling, X. Ding, Y.-H. Hu, J.-B. Zhou, X.-Y. Yang, H.-Y. Liang, W.-M. Fan, and W. Sun (2011), Mesozoic large magmatic events and mineralization in SE China: Oblique subduction of the pacific plate, *Int. Geol. Rev.*, *53*(5-6), 704–726.

White, S. M., J. A. Crisp, and F. J. Spera (2006), Long-term volumetric eruption rates and magma budgets, *Geochem. Geophys. Geosyst.*, *7*, Q03010, doi:10.1029/2005GC001002.

Zhu, G., T. Gerya, P. Tackley, and E. Kissling (2013), Four-dimensional numerical modeling of crustal growth at active continental margins, *J. Geophys. Res.*, *118*, 4682–4898, doi:10.1002/jgrb.50357.